Proceedings of the 8th European Symposium on Corrosion Inhibitors (8 SEIC)
Ann. Univ. Ferrara, N.S., Sez. V, Suppl. N. 10, 1995.

ROTATING CYLINDER VS. LOOP TESTING OF INHIBITORS FOR CO_2 CORROSION

S.NESIC*, G.T.SOLVI* AND S.SKJERVE**
* Institute for Energy Technology - Kjeller (Norway)
** Statoil - Trondheim (Norway)

ABSTRACT

A study was carried out to investigate the effect of various hydrodynamic parameters on the corrosion rate of low carbon steel in CO_2 environments in the presence of inhibitors. Two different flow geometries: rotating cylinder and pipe flow were studied simultaneously in the same electrolyte within a glass loop. The comparisons were carried out at room temperature, pH 4-6, p_{CO_2}=1 bar, v=0-13 m/s. The hydrodynamic conditions studied cover the range from static to highly turbulent flow. The corrosion process was monitored with the following electrochemical measuring techniques: polarisation resistance, potentiodynamic sweep and electrochemical impedance. The comparison of the two flow geometries was carried out in terms of hydrodynamics, mass transfer and CO_2 corrosion.

The measured mass transfer rates were found to agree well with previously published correlations for the rotating cylinder and straight pipe flow. In case of CO_2 corrosion without inhibitors it was possible to achieve good agreement between corrosion rates in the two flow geometries by having the same water chemistry and mass transfer conditions. This conclusion is valid for the case when no protective corrosion product or scale are present. With the inhibitors present the performance of both the amine and imidazoline based inhibitor measured using the rotating cylinder was identical to the one in the straight pipe flow geometry. The performance of the inhibitors was not significantly affected by the flow, in the range from 2 m/s to 10 m/s (corresponding to a shear stress of 13 Pa and 222 Pa respectively).

INTRODUCTION

Corrosion can be affected by flow differently depending on the mechanism governing the corrosion process. One can arbitrarily discriminate two major cases: (a) effect of flow on corrosion when no surface films are present and (b) effect of flow on corrosion in the presence of surface films (precipitates, inhibitors, etc.). In the no-film case the primary effect of flow on corrosion is through the mass transfer of the species involved in the corrosion reaction at the metal surface. When surface films are present they can reduce the corrosion rate by hindering the transport of species involved in the electrochemical reactions at the metal surface. In case of inhibitor films, parts of the surface are "blocked" by the inhibitor and the electrochemical double layer can be altered. The inhibitor films can be locally or globally removed by the flow, leading to very high corrosion rates. It is not yet clear which forces are responsible for mechanical film removal. In the literature, the average wall "shear stress" [1] and near-wall "turbulence fluctuations" [2] or "turbulent bursts" [3] were connected with the onset of film removal, however there is no clear and detailed study where this was investigated. The present study is aimed at studying the effect of flow on CO_2 corrosion without and with protective inhibitor films present.

EXPERIMENTAL

The glass loop

The experimental glass flow loop used in the present study is shown in Figure 1. The loop was built to handle two-phase oil/water flow. However, only the single-phase water flow experiments are presented here. Glass was selected as the main loop material for two reasons: it enables application of aggressive cleaning procedures (in between experiments with inhibitors), and because of the optical transparency (important especially in two-phase flow experiments).

Two test sections were mounted in the loop: the *straight pipe* (SP) and the *rotating cylinder* (RC). The same electrolyte was circulating through both test sections guarantying identical water chemistry conditions for the corrosion processes. The same idea was previously used by Efird et al. [4] in a similar study. The enlarged view of the SP test section made from PTFE is shown in Figure 2. Two or three steel specimen were flush mounted in the pipe (d_p=15 mm ID). Optionally up to three additional pipe test sections can be added to the existing one in series. The RC (d_c=10 mm) mounted in a cylindrical glass chamber with all the measuring equipment is shown in Figure 3.

Most of the components of the loop including the valves were made from borosilicate glass and PTFE. Some minor components (mostly fittings) were made from polypropylene, PVC, PVDF, fluoroelastomere, AISI 316, titanium grade 2 and Hastelloy C-276 steel. The construction of the loop enables reliable control of the flow parameters, water chemistry and temperature and stable and reliable automatic operation of the loop for extended periods of time (up to several weeks).

Water chemistry

Water chemistry is one of the most important factors affecting the corrosion rate so significant attention has been given to this matter. Water preparation included: water purification by destillation or reverse osmosis and bubbling with CO_2 typically for one day previous to the experiment. Continuos CO_2 bubbling was maintained throughout the experiment. The O_2 content was measured occasionally and kept below 50 ppb throughout the experiment. Addition of HCl and $NaHCO_3$ has been used to achieve the desired pH. It was possible to control the Fe^{2+} concentration by an iron generator (for increasing Fe^{2+} concentration), an ion exchanger (which can substitute the Fe^{2+} in the solution by H^+ or Na^+ ions) and a high temperature iron precipitator. When needed, samples of the loop water were taken for analysis in order to determine the amount of dissolved CO_2 and the concentration of Fe^{2+}. The pH was measured with two independent electrodes in order to register a possible drift: one was placed in a side stream taken from the main circulation circuit and the other was placed in the RC chamber. The water temperature was kept constant at the desired temperature ±1 °C.

Material

In all experiments a low carbon X65 steel was tested which is a typical pipeline steel. Chemical composition of the steel is given in Table 1.

Table 1 Chemical composition of the X65 pipeline steel used for the working electrode (mass%)

C	Mn	Si	P	S	Cr	Cu	Ni	Mo	Al	V	Sn	Ti	Nb
0.069	1.55	0.25	0.012	0.001	0.05	0.04	0.04	0.008	0.042	0.035	0.002	0.002	0.042

Inhibitor composition

Both inhibitors studied were the commercial formulations as delivered by the producer. Very little information was available on the composition of the inhibitors.

According to the producer the amine based inhibitor (ABI) is composed of 30-60% amine based fatty acid derivatives, the rest being water. An antioxidant is also present which helps in preparation of the metal surface for adsorption. The producer characterises the ABI as a single-component filming corrosion inhibitor (no surfactants present). It is believed that the amine molecules are chemically bound to the metal surface.

Even less was known on the composition of the imidazoline based inhibitor (IBI). According to the producer the IBI is composed of 10-30 % imidazoline salts and 10-30% butylglycol the rest probably being water. It is believed that imidazoline molecules are chemically bound to the metal surface and offer corrosion protection. The butylglycol is added probably as a solvent.

Corrosion measurements

The corrosion process was followed with the following electrochemical techniques: polarisation resistance, AC impedance and potentiodynamic sweep. A three electrode set-up was used in all electrochemical experiments both in the SP and the RC test section. In the SP test section (Figure 2) the working and the counter electrodes were mounted flush with the pipe wall so that minimal flow disturbance was created. The working electrodes made from carbon steel and the counter electrodes made from Hastelloy C-276 steel were identical in shape (area of 2.9 cm^2) and were mounted diametrically opposite each other so that a "uniform" current distribution was obtained during polarisation experiments. An external Ag/AgCl reference electrode (filled with saturated KCl) was connected to the cell via an ion conducting porous wooden plug.

In the RC test section, Figure 3, a carbon steel working electrode was mounted onto a rotator with a speed control unit (0-5000 rpm). The specimen was machined from the parent material into a cylinder 10 mm in diameter and 10 mm long. The exposed area of the specimen was 3.14 cm^2. A concentric platinum wire ring served as a counter electrode. An external Ag/AgCl reference electrode was connected to the cell via a Luggin capillary with a porous wooden plug. The rotating speed of the working electrode was occasionally controlled with a stroboscope. Electrochemical measurements

were made with a Gamry Instruments Inc. potentiostat with an eight channel multiplexer connected with a PC 486/25 computer.

Procedure

The glass loop was filled with approximately 56 litres of electrolyte: destilled water + 1 mass% NaCl. Then the CO_2 was continuously bubbled through the electrolyte (usually for 24 hours prior to the experiment) in order to deoxygenate and saturate the solution with carbon dioxide. Monitoring of pH and O_2 concentration was used to judge when the solution was in equilibrium. Then the pH was adjusted by adding HCl or $NaHCO_3$. Prior to immersion the carbon steel specimen surfaces were polished with 500 and 1000 grit silicon carbide paper, degreased with acetone and finally washed with alcohol. After the preparation, the samples were inserted into the loop. Subsequently polarisation resistance measurements were started. In the inhibitor experiments, the samples corroded in the loop for some time at $v_p=v_e=2$ m/s (3820 rpm) before the introduction of the inhibitor (3 hours for ABI and 19 hours for IBI). The inhibitors were added at this velocity. The polarisation resistance measurements were conducted by polarising the working electrode ±5 mV from the free corrosion potential and scanning at 0.2 mV/s. The solution resistance was measured independently using AC impedance and subtracted from the polarisation resistance. The AC impedance measurements were done by applying a sinusoidal oscillating potential to the working electrode ±5 mV_{rms} around the free corrosion potential using the frequency range 10 mHz - 100 kHz. At the end of each experiment the potentiodynamic sweeps were conducted, starting 300-600 mV below and finishing 150-200 mV over the free corrosion potential. Typical scanning rate used was 0.2 mV/s.

Difficulties

Numerous difficulties followed the experimental program. Our experience might be instructive for other researchers in this area. We found that even very small quantities of contamination leaking from loop components could be detrimental and lead to erroneous measurements. During our experiments we encountered contamination with lead dissolving from a minute seal in a rotameter used to monitor the flow rate through a bypass stream. It was also found that tin was dissolving from a graphite pump bearing. In both cases the contaminating metals were deposited on the surface of our specimen. The most serious contamination was discovered to come from a short nitrile rubber hose used to connect the water pump with the loop. The mysterious contaminant was a very effective corrosion inhibitor in itself. When the experiments with

inhibitors were started another problem appeared. It seemed as there was an additional contaminant in the loop which did not affect the base-line corrosion rate but affected the performance of the inhibitor. In other words: our inhibitor was "inhibited". The source of this contamination in the loop was particularly difficult to discover. After an in-depth investigation it was discovered by SEM and X ray analysis that the source of the problem was a very thin layer of molybdenum (probably as an oxide) present on the surface of our specimen which prevented the inhibitor from adsorbing. The source of the molybdenum were a few minor components of the loop (fittings and small tubes) made from stainless AISI 316 steel. During the washing of the loop between the experiments, when HCl solution was used, the protective passive layer on the AISI 316 steel was destroyed and molybdenum began dissolving. All previously mentioned sources of contamination had to be removed before meaningful measurements were made.

RESULTS AND DISCUSSION

Selection of an adequate laboratory scale apparatus for testing of flow effects in CO_2 corrosion is a difficult task. The selected experimental set-up must have well defined hydrodynamic and mass transfer characteristics. In addition, good control of water chemistry must be possible. The *straight pipe* and the *rotating cylinder* test sections used in the present experiments satisfy both previous requirements. By testing the two flow geometries using the same electrolyte we could assume that the water chemistry was identical. This enabled us to concentrate on the differences in the CO_2 corrosion process that arise from hydrodynamic and mass transfer considerations.

Fluid flow

From a practical point of view we are primarily interested in turbulent flow regimes. For pipe flow at Reynolds numbers below $Re_p = \rho v_p d_p/\mu = 2000$ laminar flow is encountered. For $2000<Re_p<3000$ transition to turbulent flow occurs. Translated to our experimental conditions (d_p=15 mm ID, T=20°C) turbulent flow was achieved for all velocities larger than 0.2 m/s. At higher temperatures the transition occurs at even lower velocities. For a RC geometry laminar flow is typically encountered for Reynolds numbers $Re_c = \rho v_c d_c/\mu < 200$ (where $v_c = \omega d_c/2$ is the peripheral velocity of the RC). This means that in our conditions (d_c=10 mm, T=20°C) already for rotation speeds larger than $\omega = 40$ rpm turbulent flow was encountered in the vicinity of the cylinder. This corresponds to a RC peripheral velocity of v_c=0.02 m/s. The shear stress

exerted at the wall in pipe flow can be determined from the pressure gradient along a pipe:

$$\tau_w = \frac{\Delta p}{\Delta L}\frac{d_p}{4} \tag{1}$$

However, we did not measure the pressure drop in the experiments so the shear stress had to be determined from existing correlations. For turbulent pipe flow such a relationship can be found only empirically in terms of *laws of friction*. One of the well known such correlations for high Reynolds numbers ($Re_p > 10^5$) is the Coolebrook equation [5]:

$$\frac{1}{\sqrt{f_p}} = -4\log\left(\frac{\varepsilon}{3.7d_p} + \frac{1.256}{Re_p\sqrt{f_p}}\right) \qquad \text{for } Re_p > 3000 \tag{2}$$

For the rotating cylinder in the case of a turbulent flow regime (smooth surfaces) the friction factor is [6]:

$$f_c = 0.158\,Re_c^{-0.3} \qquad \text{for } Re_c > 300 \tag{3}$$

In Figure 4 the calculated shear stress is compared for SP and RC flow for our loop at 20°C. The velocity plotted on the x-axis is the average cross-section velocity ($v_p = Q_p/A_p$) for SP flow and the peripheral velocity ($v_c = \omega d_c/2$) for the RC. The smooth surface correlations were used to calculate the shear stress. This is justifiable as in our experiments the surface roughness varied from $\varepsilon/d_p \approx 1\times10^{-4}$ for the freshly polished specimens to $\varepsilon/d_p \approx 4\times10^{-4}$ for heavily corroded surfaces (determined by looking at surface cross sections using SEM). Calculated from the previous correlations, even for the highest velocities the effect of maximum roughness on shear stress was less than 10%.

From Figure 4 it can be seen that with the RC, shear stresses up to 25 Pa could be achieved at maximum rotation speed (5000 rpm what corresponds to v_c=2.61 m/s). In the SP as much as 300 Pa was achieved at v_p=13 m/s. For the "equivalent" velocity (v_p=v_c) similar shear stress is obtained for the two flow geometries. This is true only

when the RC and SP diameters are of the same order of magnitude what is the case in our loop. We did most of our experiments at 2 m/s where the calculated shear stress was 16 Pa and 12 Pa for the RC and the SP respectively.

Mass transfer

According to the general understanding of the CO_2 corrosion mechanisms, mass transfer is important primarily at pH<5 when it affects the limiting current for H^+ reduction. Since this pH range is in the domain of our interest, mass transfer characterisation of the two flow geometries in our loop was done. This was achieved by conducting experiments at pH 3 in a 1% NaCl-water solution purged with N_2 gas. Under these conditions the dominant cathodic reaction for modest overpotentials (η < -0.5 V) is the reduction of H^+ ions. For the overpotentials between -0.2 and -0.5 V it is possible to obtain clear mass transfer limiting currents as shown in Figure 5. Potentiodynamic sweeps were conducted beginning from the corrosion potential and finishing 0.8 V below. This was repeated for different SP velocities and RC speeds. The measured limiting currents were converted to mass transfer coefficients by using:

$$k_m = \frac{i^d_{lim(H^+)}}{F \cdot e^{-pH}} \tag{4}$$

Mass transfer coefficients for turbulent flow are well established in the literature for the two flow geometries under investigation. In the case of straight pipe flow the correlation of Berger and Hau [7] can be used:

$$Sh_p = \frac{k_m d_p}{D} = 0.0165 \cdot Re_p^{0.86} \cdot Sc^{0.33} \tag{5}$$

For the rotating cylinder flow the correlation of Eisenberg et al. [8] is appropriate:

$$Sh_c = \frac{k_m d_c}{D} = 0.0791 \cdot Re_c^{0.7} \cdot Sc^{0.356} \tag{6}$$

The measured and calculated mass transfer coefficients as a function of velocity are shown in Figure 6. The value $D_{(H^+)} = 9.31 \times 10^{-9}\, m^2/s$ has been used to obtain the k_m

from the Sherwood number [9]. In Figure 6 we have again arbitrarily selected to compare the k_m for the "equivalent" velocity (v_p=v_c). However, the most important conclusion is that both for the RC flow and for the SP flow the agreement between the measured mass transfer coefficient in our loop and the one predicted using the previous correlations is good. This means that good control of the mass transfer conditions was achieved in the loop for both flow geometries. Somewhat larger discrepancy between predicted and measured k_m was obtained for the SP flow. We can assume that our working electrodes in the SP test section (Figure 2) which were only 20 mm long ($1.33 \times d_p$) were somewhat too short to completely eliminate the effect of developing mass transfer boundary layers.

As a general case one can calculate an equivalent velocity in the pipe and a cylinder [10, 11] which guaranties identical mass transfer conditions. This can be done by equating (5) and (6), using that $(k_m)_p$=$(k_m)_c$ and substituting the appropriate expressions for the Schmidt number and the Reynolds number . This gives the following expression:

$$v_c = 0.1066 \cdot \left(\frac{\rho}{\mu}\right)^{0.266} \cdot D^{0.0371} \cdot \left(\frac{d_c^{0.429}}{d_p^{0.200}}\right) \cdot v_p^{1.229} \qquad (7)$$

This equation as well as our mass transfer measurements enabled us to select the velocity in the SP and the corresponding rotating speed for the RC which gave identical mass transfer rates for the two geometries. In our case we found that by selecting v_p=v_c=2 m/s we measured practically identical mass transfer coefficients $(k_m)_p = (k_m)_c = 4 \times 10^{-4}$ m/s at 20°C. This is approximately in the middle of the region where the two curves overlap (Figure 6). The majority of the conducted corrosion experiments presented below were done at v_p=v_c=2 m/s (3820 rpm) where the mass transfer conditions were approximately equal.

CO_2 corrosion

Corrosion experiments without inhibitors. The corrosion experiments were carried out at room temperature (20 - 22°C) at pH 4, pH 5 and pH 6. The velocity was varied from stagnant to 13 m/s. Experiments were started by measuring the polarisation resistance (corrosion rate) every 30 min at v_p=v_c=2 m/s (equivalent mass transfer conditions). Typically 24 hours after the beginning of the experiments measurements of the polarisation resistance (corrosion rate) and the corrosion potential as a function of the velocity were performed. The velocity was varied from zero to 13 m/s and back

in the SP section and from zero to 5000 rpm and back in the RC chamber. All this was performed within about 2-5 hours.

Subsequently the velocity was adjusted back to v_p=v_c=2 m/s. After a waiting period of 12 hours (in order to obtain stable corrosion rates) AC impedance measurements were conducted. Finally, potentiodynamic sweeps were done and the specimen were taken out from the loop and prepared for the SEM analysis.

The potentiodynamic sweeps measured at v_p=v_c=2 m/s (equivalent mass transfer conditions) and different pH are shown in figure 7. The measured curves are overlaid with theoretical curves predicted with the model of Nesic et al. [12] for easier interpretation of the corrosion mechanisms. The data obtained for the RC electrode are in good agreement with the data from the SP section over the whole potential range for all three pH. At pH 4 one can see the large contribution of the H^+ reduction reaction which is diminished at pH 5 and completely disappears from the picture at pH 6. At pH 5 and pH 6 the dominant cathodic reaction at the corrosion potential is direct H_2CO_3 reduction and for higher negative overpotentials H_2O reduction. Good agreement between the RC and SP measurements is clear for all three cathodic reactions as well as for the anodic reaction. This leads us to a conclusion that the mechanism of the CO_2 corrosion in the two flow geometries (RC and SP) is the same at 20°C. It is then not difficult to understand that measured corrosion rates shown in Figure 9 were very similar for the two geometries.

The potentiodynamic sweeps as well as the LPR-measurements have been corrected for the solution resistance found by the AC impedance technique. In Figure 8 results of the AC impedance measurements (Nyquist plot) at 20°C, pH 6, v_p=v_c=2 m/s are shown. A good agreement between the measured polarisation resistance values for the RC and SP geometry is shown. When one takes into account the difference in area for the two sample geometries (10% larger for the RC), the measured polarisation resistances in Ωm^2 for the two geometries are even closer. The similar shape of the measured curves confirms that an identical mechanism of CO_2 corrosion was present in both flow geometries.

The obtained corrosion rates as a function of velocity at 20°C are shown in Figure 9 for the different pH. The corrosion current is shown on the left and the corresponding corrosion rate on the right hand side (for iron dissolution the relation 1 mm/y =1.155 A/m^2 was used). In Figure 9 the results were corrected for the effect of the presence of oxygen, by subtracting the contribution of the oxygen reduction current. Measured

oxygen concentration varied from 10-40 ppb in the different experiments. Previously shown mass transfer correlations and the diffusion coefficient $D_{O_2} = 2.09 \times 10^{-9}\ m^2/s$ at 20°C was used to calculate the limiting current for oxygen reduction. The B value was calculated for different conditions using the model of Nesic et al. [12]

The corrosion rates at static conditions are approximately the same for all three pH values, shown in Figure 9. As the velocity is increased, the limiting current for H^+ reduction increases leading to an increased overall cathodic reaction and higher corrosion rate. The increase of the corrosion rate with velocity is most pronounced at pH 4 where the concentration of H^+ is highest.

Since it was noticed that a good agreement was obtained for the corrosion rates of the RC and SP specimen, this suggests that in the absence of surface films one can obtain identical corrosion rates by setting equivalent water chemistry and mass transfer conditions at the two flow geometries. It also confirms that in this case the present understanding of CO_2 corrosion mechanisms permits us to transfer the data from one flow system to another. In Figure 10, SEM images of the cross sections of specimens exposed for 63 hours at 20°C, pH 5 is shown. Evenly attacked surfaces virtually free of any films can be observed.

Corrosion experiments with inhibitor. Tests where measurements were simultaneously conducted in the SP and RC test sections were done to check if a bench size apparatus (e.g. glass cell with a rotating cylinder) could be successfully used for testing of corrosion inhibitors. The velocity in the SP test section was maintained at v_p=2 m/s, while the RC electrode was rotating at 3820 rpm (v_c=2 m/s). As previously demonstrated this guaranties the same mass transfer conditions and a similar shear stress in the two test sections. After addition of the inhibitor at v_p=v_c=2 m/s, the corrosion rate was reduced in both the RC and SP test sections to a low value for both inhibitors as shown in Figure 12 and Figure 16. The kinetics of the reduction of the corrosion rate was identical for both geometries and so was the steady state corrosion rate. This finding was confirmed by looking at the potentiodynamic sweep measurements shown in Figure 13 and Figure 17 and the AC impedance measurements shown in Figure 14 and Figure 18. Similar conclusion was reached by Chesnut and Choi [13] who found good agreement between a rotating cylinder and straight pipe flow when testing inhibitors at the same shear stresses.

The effect of extreme flow conditions on CO_2 corrosion in the presence of inhibitors was studied by varying the velocity from 2 m/s to 10 m/s corresponding to a shear

stress of 12 Pa and 222 Pa respectively. Results are shown in Figure 11 for an experiment conducted with 30 ppm of ABI at pH 4, T=21°C and 1 bar CO_2. When the velocity was changed from 2 m/s to 10 m/s and back, only a small change in the corrosion rate was obtained. The variation can be explained with an increased rate of mass transfer for the H^+ ions (cathodic reactants). However, it can be concluded that the performance of the ABI inhibitor was not significantly affected by the flow, as the observed variations are within the margin of experimental error. Similar behaviour was found for the IBI inhibitor as shown in Figure 15. This conclusion cannot be generalised as it is possible that different inhibitors can show very different behaviour under extreme flow conditions [3, 13, 14]. It is also possible that addition of inhibitor at high velocity could lower it's ability to film the steel surface. This should be tested out at a later stage.

CONCLUSIONS

In case of CO_2 corrosion without the presence of inhibitors:

- Good agreement was obtained between the measured mass transfer coefficients and the ones predicted using the correlation of Berger and Hau [7] for straight pipe flow and the correlation of Eisenberg et al. [8] for the rotating cylinder flow geometry. This enabled us to select a velocity in the pipe and the corresponding rotating speed for the rotating cylinder which gave approximately equal mass transfer conditions for the two geometries.
- It is possible to achieve the same mechanism and obtain approximately the same rate of the CO_2 corrosion process on a rotating cylinder as on a straight pipe electrode by setting identical water chemistry and mass transfer conditions at the two flow geometries.

When protective inhibitor films were present at the surface:

- The performance of both the amine and imidazoline based inhibitors measured using the rotating cylinder was identical to the performance measured in the straight pipe flow geometry.
- The performance of the inhibitors was not significantly affected by the flow, in the range from 2 m/s to 10 m/s (corresponding to a shear stress of 12 Pa and 222 Pa respectively).

NOMENCLATURE

A	area, m^2;
d_p, d_c	pipe and cylinder diameter, m;
D	diffusion coefficient, m^2/s ;
$f = 2\tau_w/\rho v^2$	Fanning friction factor;
F	Faraday constant (96490 C/equiv.);
i	current density, A/m^2 ;
i_{lim}^d	diffusion limiting current density, A/m^2 ;
k_m	is the mass transfer coefficient, m/s ;
l	characteristic length, m;
L	pipe length, m;
P	pressure, bar;
p	partial pressure, bar;
Q	volumetric flow rate, m^3/s;
R	universal gas constant (8.3143 J/(mol K));
$Re = \rho v l/\mu$	Reynolds number ;
$Sc = \mu/\rho D$	Schmidt number;
$Sh = k_m l/D$	Sherwood number ;
T	temperature, °C ;
v	velocity, m/s ;

Greek symbols

ε	pipe roughness, m;
η	overpotential (applied potential - open circuit potential)
μ	viscosity, kg/(m s) ;
ρ	density, kg/m^3 ;
τ_w	wall shear stress, Pa;
ω	rotation (angular) speed, rad/s;

Subscripts

p	pipe;
c	cylinder.

REFERENCES

1. K. D. Efird, Corrosion, 33 (1977): p.3.
2. S. Nesic, J. Postlethwaite, Corrosion, 46 (1990): p.874.
3. J. L. Dawson, C. C. Shih, R. G. Miller, J. W. Palmer, "Inhibitor evaluations under controlled hydrodynamic shear", Corrosion/90, paper no. 14, (Houston, TX: NACE International, 1990).
4. K. D. Efird, E. J. Wright, J. A. Boros, T. G. Hailey, "Experimental Correlation of Steel Corrosion in Pipe Flow with Jet Impingement and Rotating Cylinder Laboratory Tests", Corrosion/93, paper no. 91, (Houston, TX: NACE International, 1993).
5. Perry's Chemical Engineers' Handbook, Sixth Edition (New York: McGraw-Hill, 1984).
6. D. R. Gabe, F. C. Walsh, Journal of Applied Electrochemistry, 13 (1983): p.3.
7. F. P. Berger and K.-F. F.-L Hau, Int. J. Heat Mass Transfer, 20 (1977): p.1185.
8. M. Eisenberg, C. W. Tobias and C. R. Wilke, J. Electrochem. Soc., 101 (1954): p. 306.
9. Atkins, P. W., Physical Chemistry, Second Edition, (Oxford, UK: Oxford University Press, 1982): p.905.
10. V. E. Heitz, Werkstoffe und Korrosion, (1964): p.63.
11. T. Chen, A. A. Moccari, D. D. Macdonald, "The Development of Controlled Hydrodynamic Techniques for Corrosion Testing", Corrosion/91, paper no. 292, (Houston, TX: NACE International, 1991).
12. S. Nesic, J. Postlethwaite, S. Olsen, "An Electrochemical Model for Prediction of CO_2 Corrosion", Corrosion/95, paper no. 131, (Houston, TX: NACE International, 1995).
13. G. Chesnut, H. J. Choi, "Laboratory Testing and Selection of Corrosion Inhibitors for Continuos Application in Multiphase Pipelines", Corrosion/94, paper no. 35, (Houston, TX: NACE International, 1994).
14. G. Schmitt, T. Simon, R. H. Hausler, "CO_2 Erosion Corrosion and its Inhibition Under Extreme Shear Stress, 1. Development of Methodology", Corrosion/90, paper no. 22, (Houston, TX: NACE International, 1990).

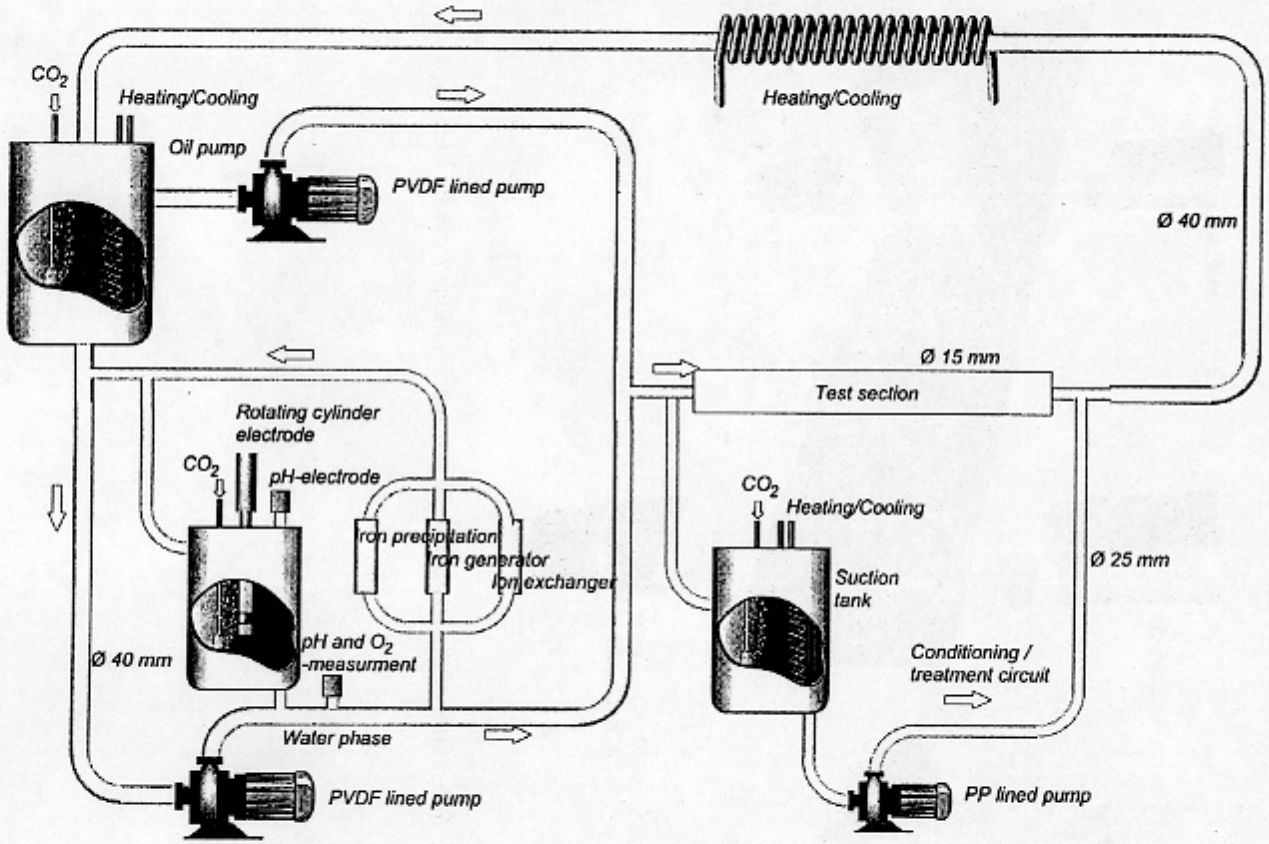

Figure 1. Schematic of the glass flow loop.

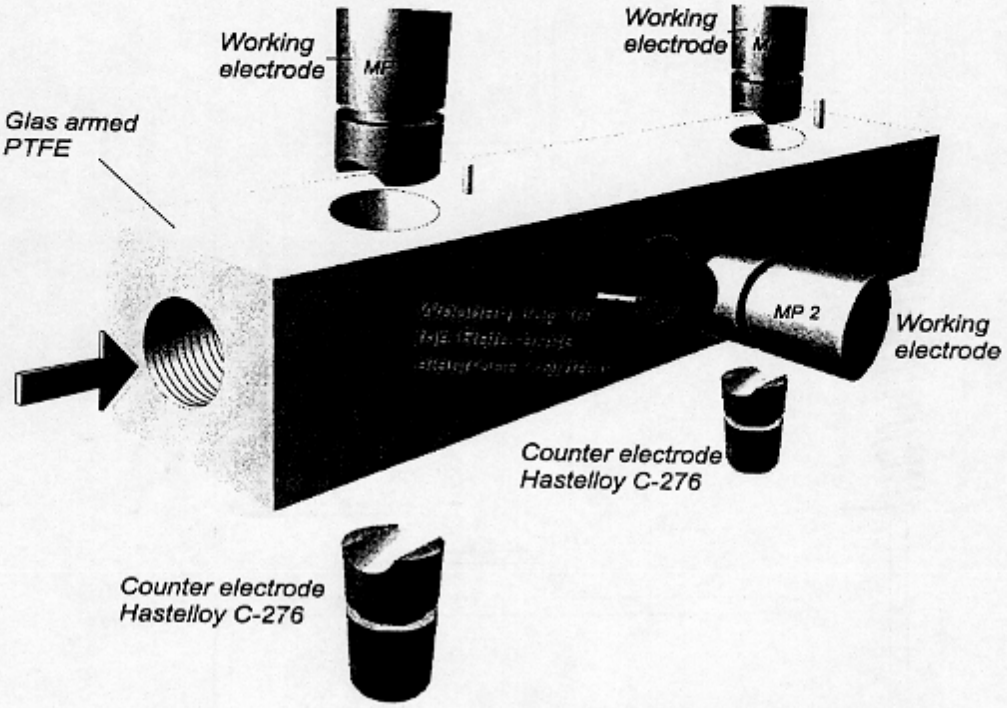

Figure 2. Schematic of the straight pipe test section made from PTFE.

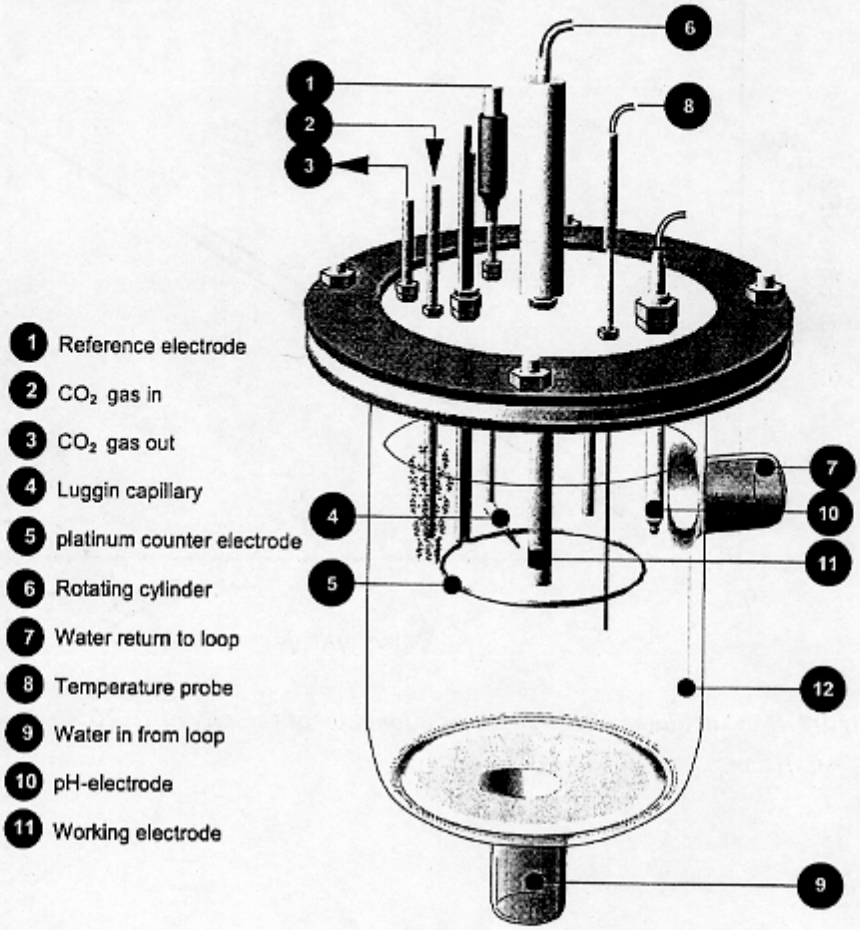

Figure 3. Schematic of the rotating cylinder test section made from glass.

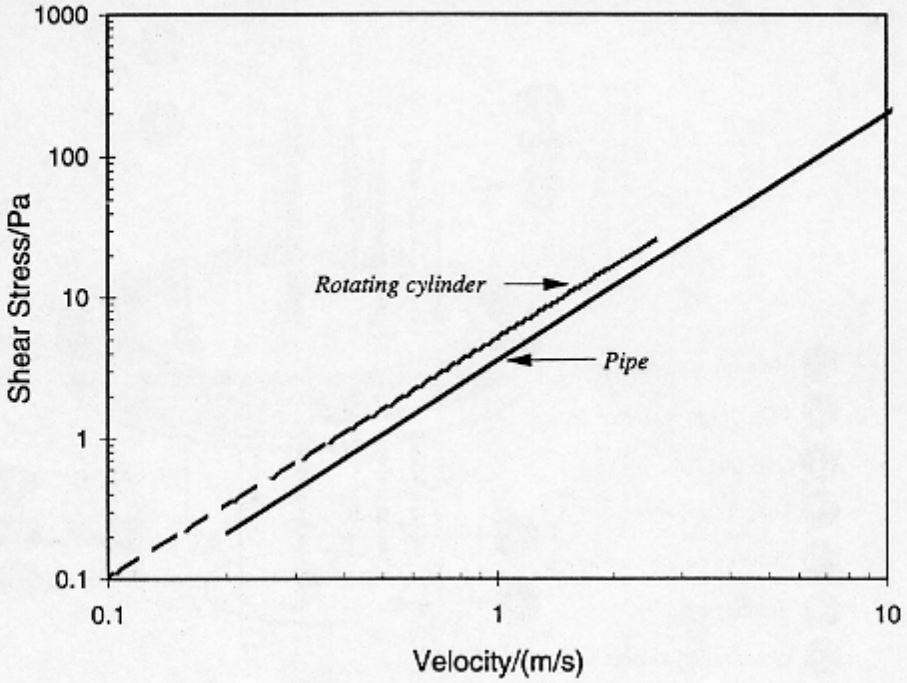

Figure 4. Calculated shear stress as a function of velocity at T=20°C. d_c *=0.01 m,* d_p *=0.015 m.*

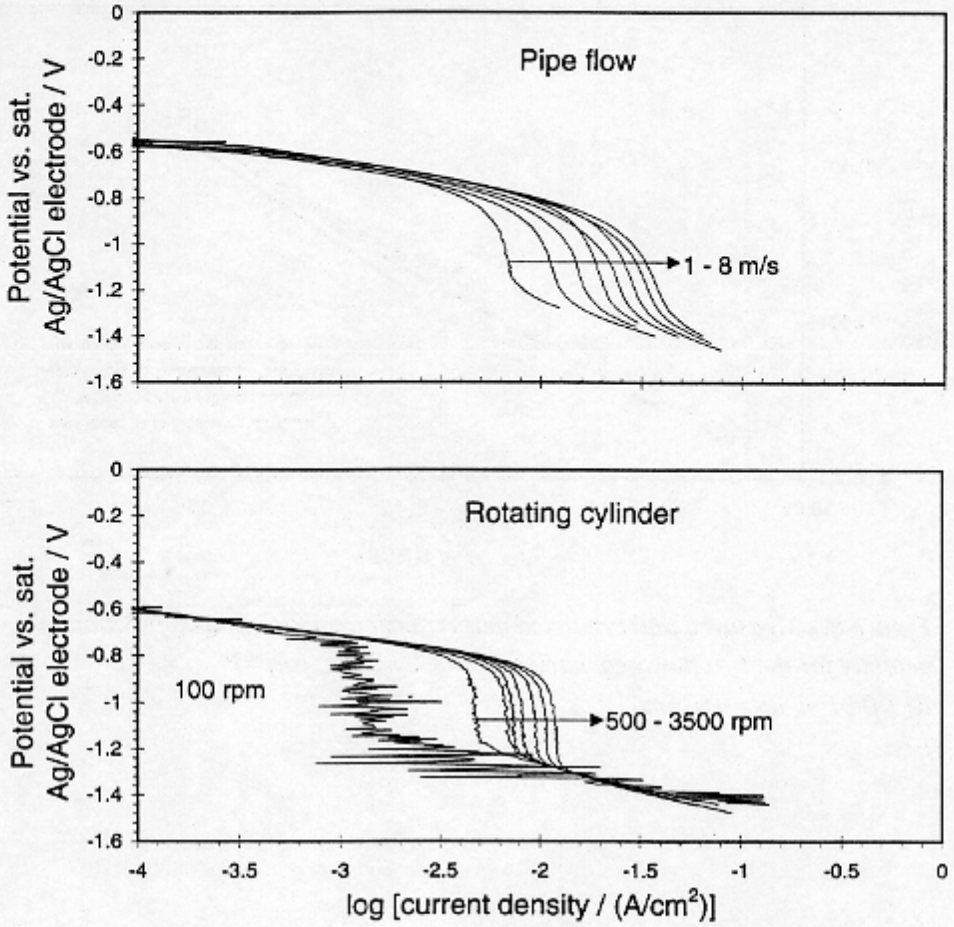

Figure 5. Potentiodynamic sweep. The effect of velocity on mass transfer limiting currents. pH=3, T=20°C, $p_{N_2} = P_{total} = 1$ bar, $d_c = 0.01$ m, $d_p = 0.015$m.

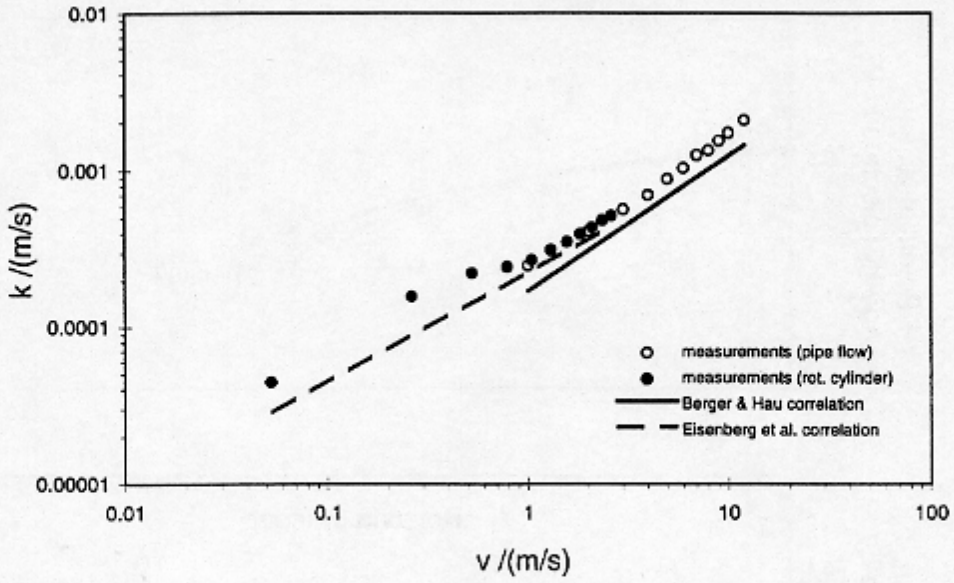

Figure 6. Measured and predicted mass transfer coefficient as a function of velocity for the two flow geometries. pH=3, T=20°C, $p_{N_2} = P_{total} = 1$ bar, $d_c = 0.01$ m, $d_p = 0.015$m.

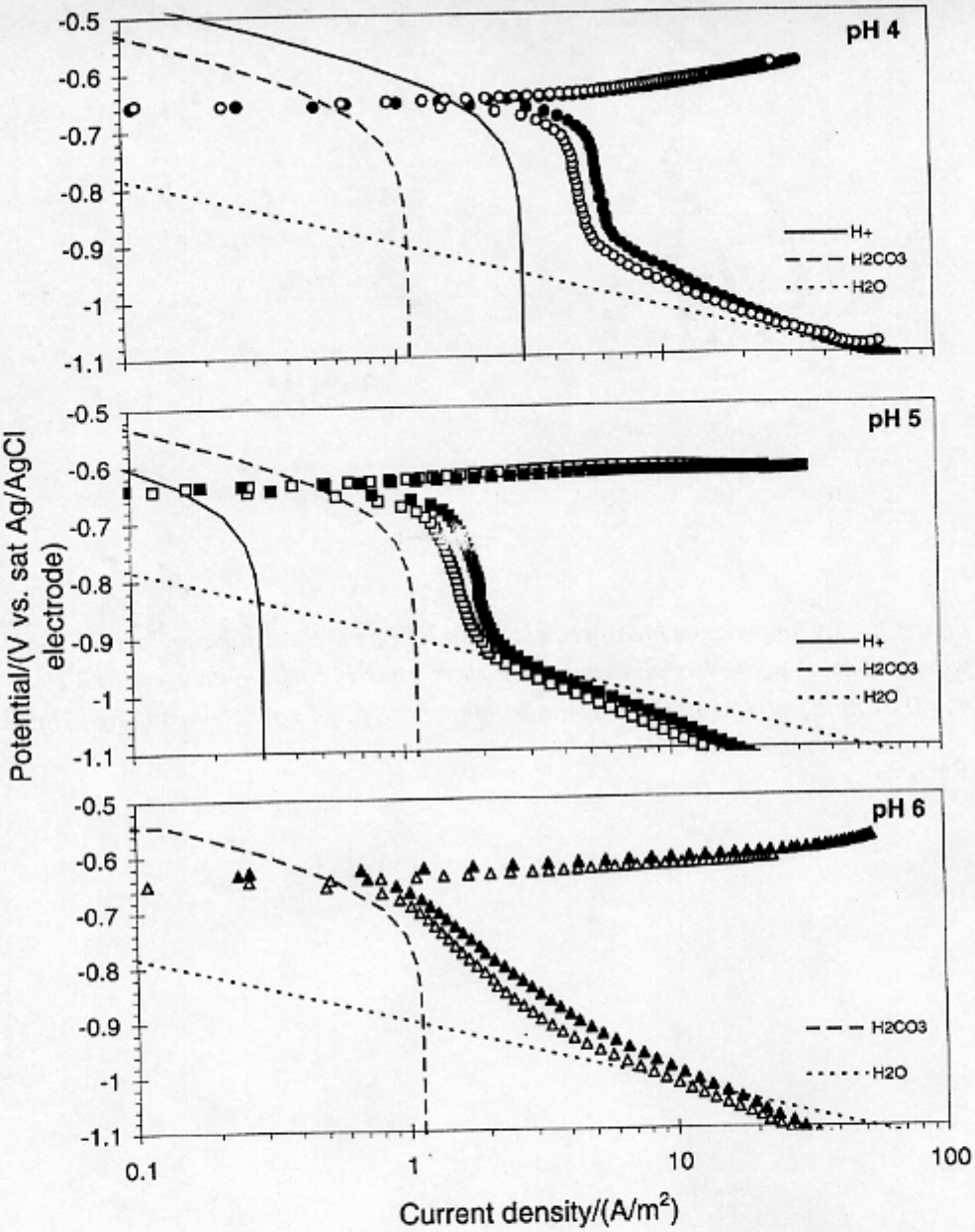

Figure 7. Potentiodynamic sweeps for different pH values conducted at T=20°C and equivalent mass transfer conditions: $v_p = v_c = 2$ m/s (3820 rpm). 1% NaCl solution, $p_{CO_2} = 1$ bar, $P_{total} = 1$ bar, $d_c = 0.01$ m, $d_p = 0.015$m. Open symbols - pipe flow, filled symbols - rotating cylinder.

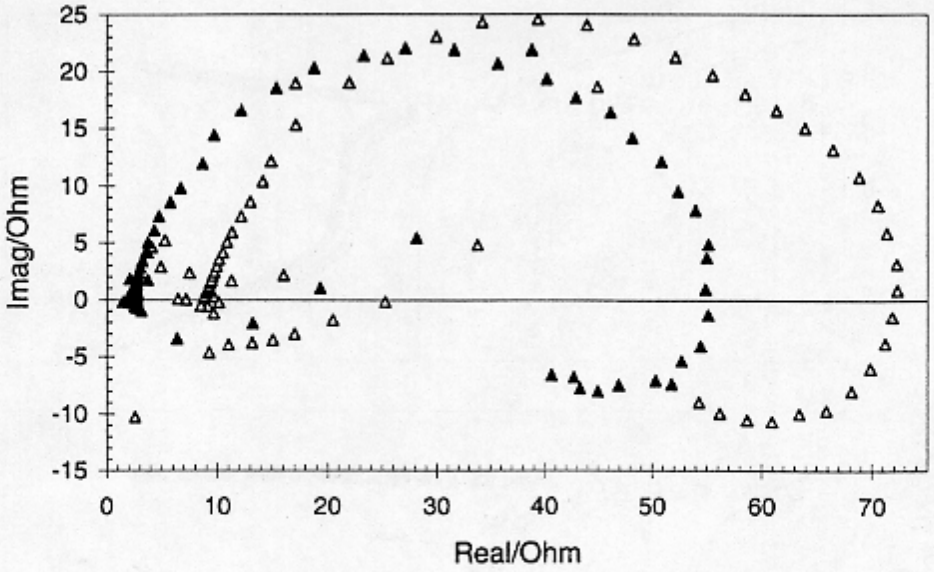

Figure 8. AC impedance measurement at T=20°C, 1% NaCl solution, pH 6, p_{CO_2}=1 bar, P_{total}=1 bar and equivalent mass transfer conditions: $v_p = v_c$ =2 m/s. d_c=0.01 m, d_p=0.015m. Open symbols - pipe flow, filled symbols - rotating cylinder.

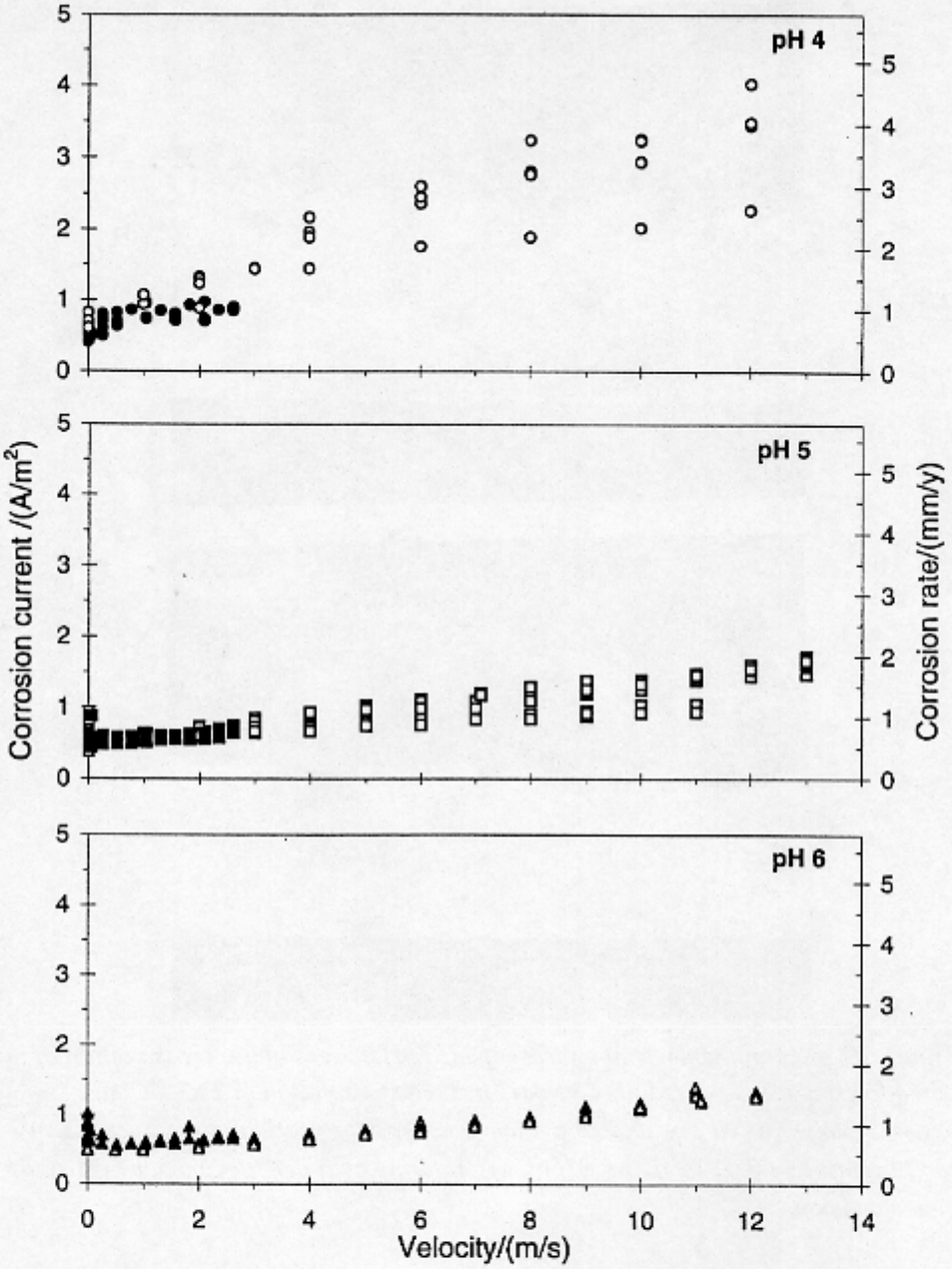

Figure 9. Effect of velocity on the corrosion rate at different pH values at T=20°C. 1% NaCl solution, p_{CO2}=1 bar, P_{total}=1 bar, d_c=0.01 m, d_p=0.015m. Open symbols - pipe flow, filled symbols - rotating cylinder.

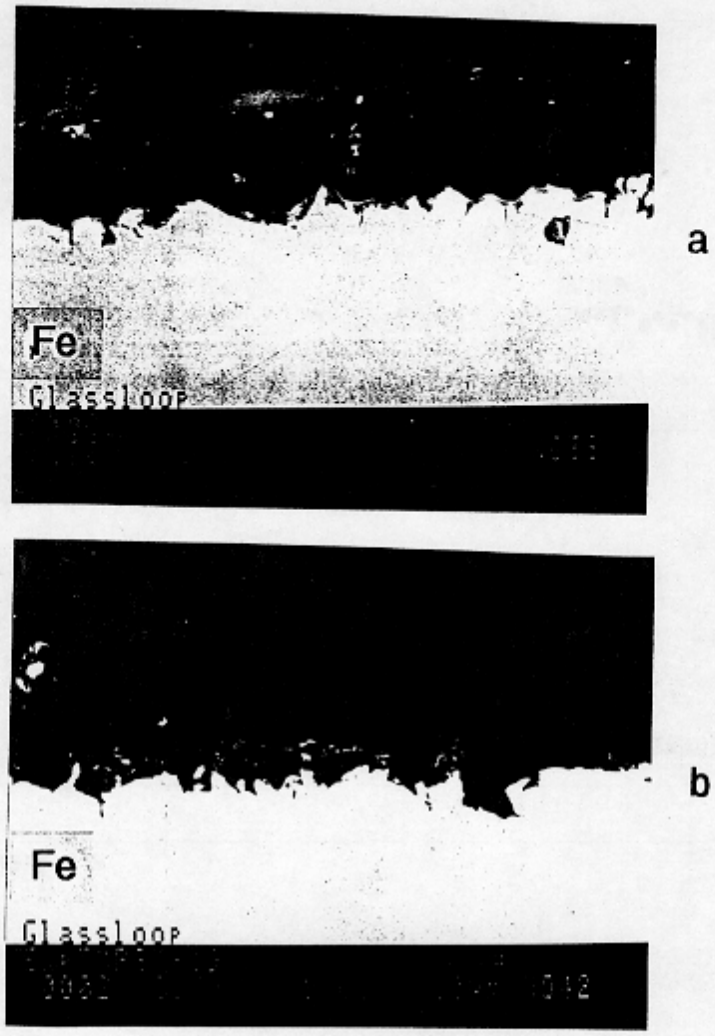

Figure 10. Scanning electron microscope (SEM) images of the cross section of the corroded surfaces exposed for 63 hours in 1%NaCl solution at T=20°C, pH 5, p_{CO_2}=1 bar, P_{total}=1 bar and equivalent mass transfer conditions: $v_p = v_c$=2 m/s (3820 rpm). d_c=0.01 m, d_p=0.015m. a) - rotating cylinder specimen, b) - straight pipe specimen.

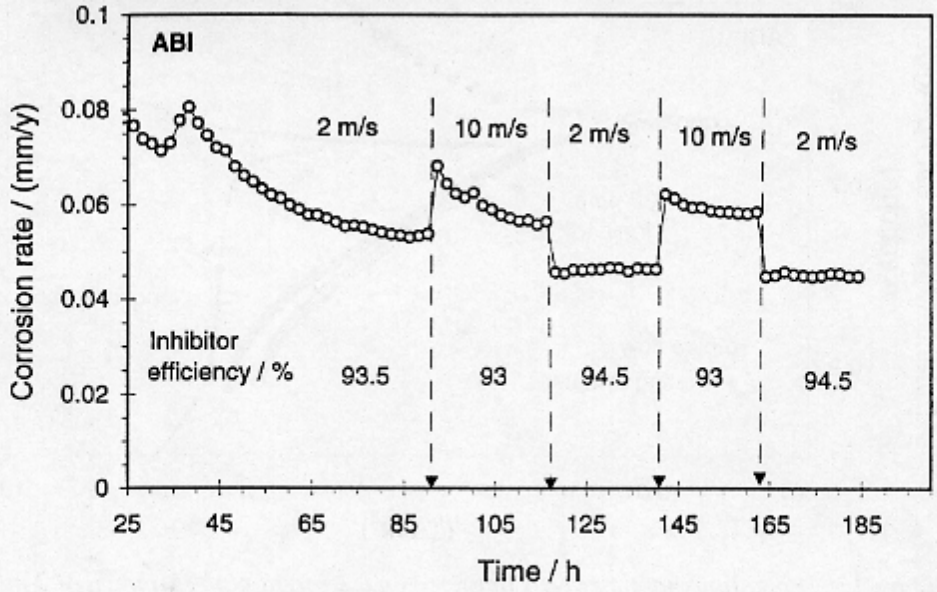

Figure 11. Effect of pipe flow velocity on the corrosion rate in the presence of 30 ppm of an amine based inhibitor. 1% NaCl solution, pH 4, T=21°C, p_{CO_2}=1 bar, P_{total}=1 bar, d_p=0.015 m.

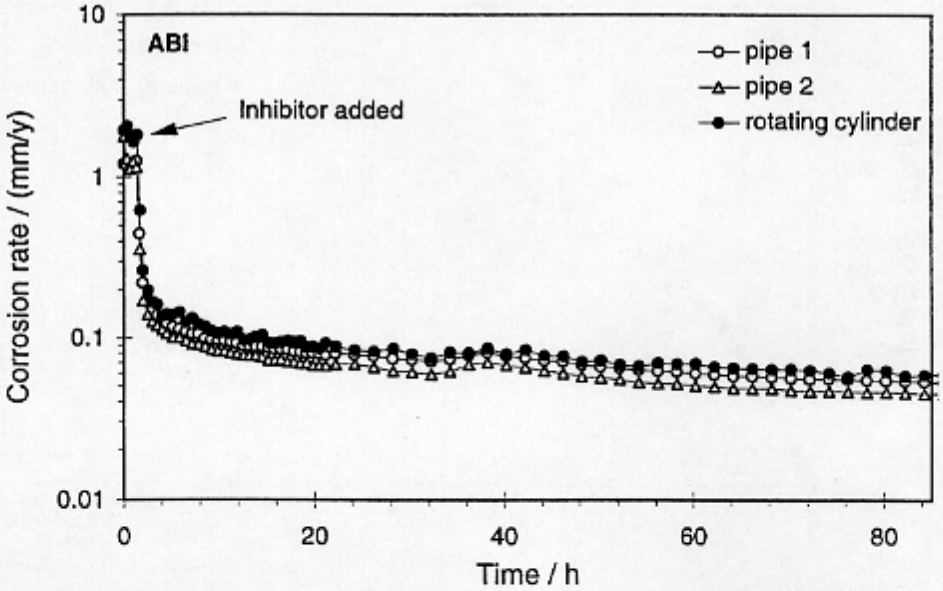

Figure 12. Comparison of the effect of 30 ppm of an amine based inhibitor on the corrosion rate for the straight pipes specimens at 2 m/s and the rotating cylinder specimen at 3830 rpm. T=21°C, pH 4, 1% NaCl solution, p_{CO_2}=1 bar, P_{total}=1 bar, d_c=0.01 m, d_p=0.015 m.

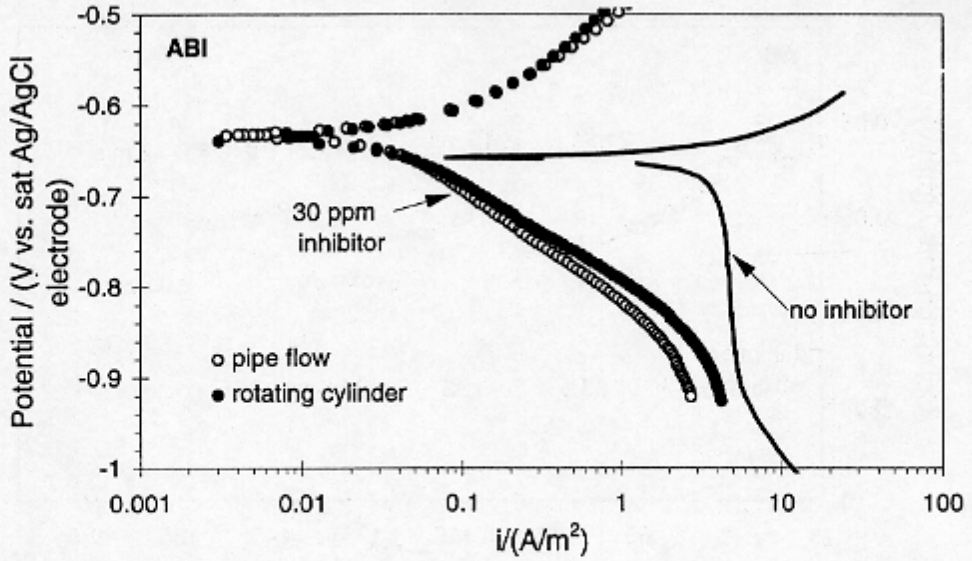

Figure 13. Potentiodynamic sweeps obtained on a straight pipe specimen at 2 m/s and a rotating cylinder specimen at 3830 rpm with and without the presence of an amine based inhibitor. 1% NaCl solution, pH 4, T=20°C, $p\,co_2$ =1 bar, P_{total} =1 bar, d_c =0.01 m, d_p =0.015 m. Scan rate 0.2 mV/s.

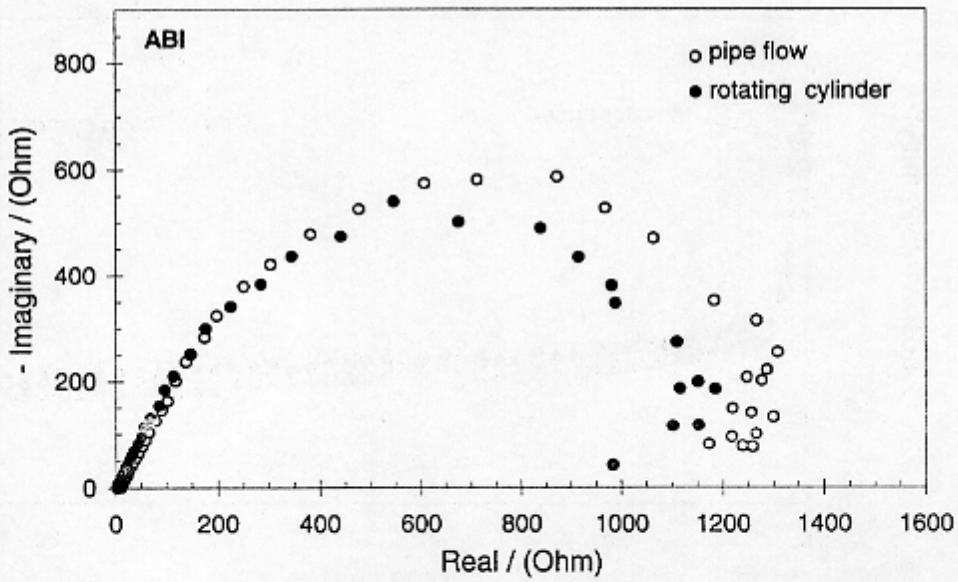

Figure 14. Comparison of the AC measurements obtained on a straight pipe specimen at 2 m/s and a rotating cylinder specimen at 3830 rpm in the presence of 30 ppm of an amine based inhibitor. 1% NaCl solution, T=21°C, pH 4, $p\,co_2$ =1 bar, P_{total} =1 bar, d_c =0.01 m, d_p =0.015 m.

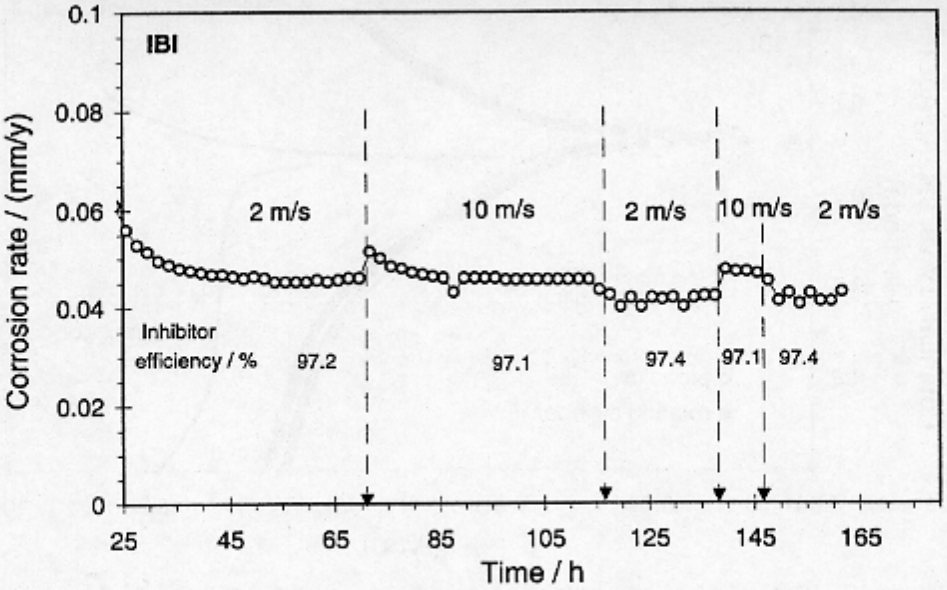

Figure 15. Effect of pipe flow velocity on on the corrosion rate in the presence of 20 ppm of an imidazoline based inhibitor. 1% NaCl solution, pH 4, T=20°C, $p\,co_2$ =1 bar, P_{total} =1 bar, d_p =0.015 m.

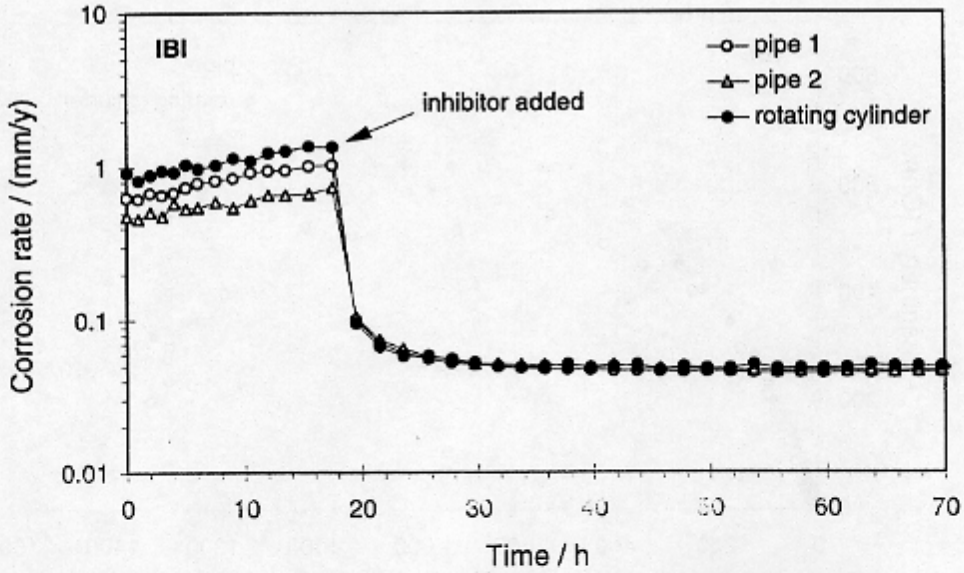

Figure 16. Comparison of the effect of 20 ppm of an imidazoline based inhibitor on the corrosion rate for the straight pipe specimens at 2 m/s and the rotating cylinder specimen at 3850 rpm. 1% NaCl solution, T=20°C, pH 4, $p\,co_2$ =1 bar, Ptotal=1 bar, d_c =0.01 m, d_p =0.015 m.

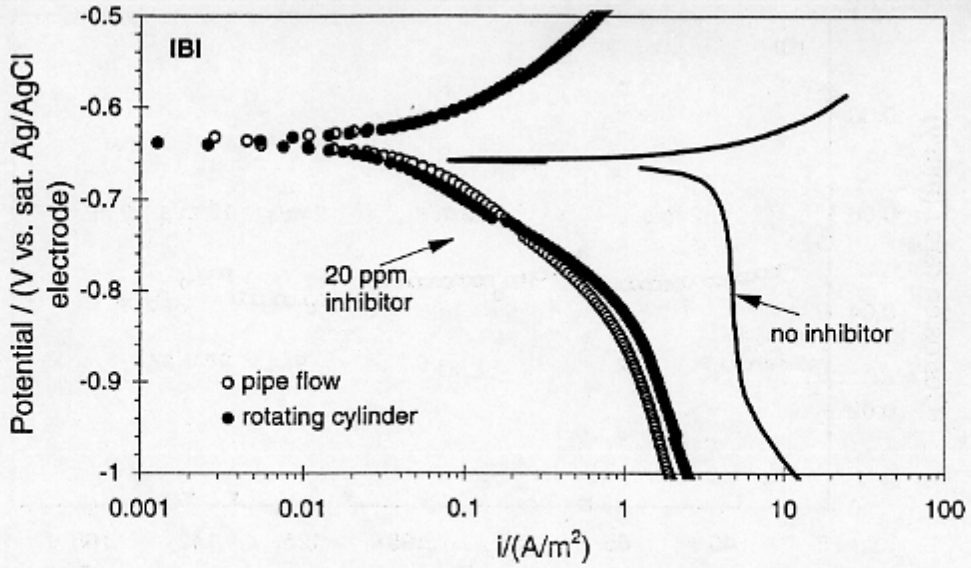

Figure 17. Potentiodynamic sweeps obtained on a straight pipe specimen at 2 m/s and a rotating cylinder specimen at 3820 rpm with and without the presence of an imidazolin based inhibitor. 1% NaCl solution, pH 4, T=20°C, p_{CO_2}=1 bar, P_{total}=1 bar, d_c=0.01 m, d_p=0.015 m. Scan rate 0.2 mV/s.

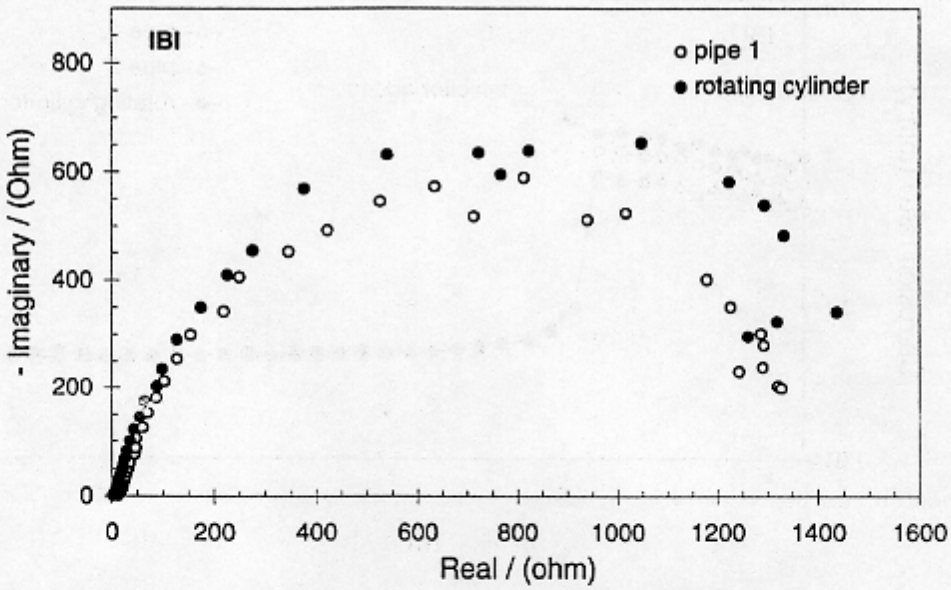

Figure 18. Comparison of the AC measurements obtained on a straight pipe specimen at 2 m/s and a rotating cylinder specimen at 3820 rpm in the presence of 20 ppm of an imidazoline based inhibitor. 1% NaCl solution, T=20°C, pH 4, p_{CO_2}=1 bar, P_{total}=1 bar, d_c=0.01 m, d_p=0.015 m.